

Scalable quantum simulation of pulsed entanglement and Einstein-Podolsky-Rosen steering in optomechanics

S. Kiesewetter, Q. Y. He, P. D. Drummond,^{*} and M. D. Reid*Centre for Quantum and Optical Science, Swinburne University of Technology, Melbourne, Australia*

(Received 23 December 2013; published 6 October 2014)

We demonstrate a complete, probabilistic quantum dynamical simulation of the standard nonlinear Hamiltonian of optomechanics, including decoherence at finite temperatures. Robust entanglement of a photonic pulse with a mechanical oscillator is predicted. Our exact quantum simulations use the positive- P technique, are scalable to large Hilbert spaces, and give excellent agreement with recent experiments. We predict the required conditions for the next stage in this research. Strong quantum steering between the photonic and mechanical systems is possible, depending on thermal occupation. This is more viable in optical than in electromechanical experiments.

DOI: [10.1103/PhysRevA.90.043805](https://doi.org/10.1103/PhysRevA.90.043805)

PACS number(s): 42.50.Wk, 03.67.Bg, 03.67.Mn, 42.50.Ct

I. INTRODUCTION

Optomechanical oscillators provide fundamental tests of mesoscopic quantum mechanics and have potential technological applications for ultrasensitive measurement. Impressive success in cooling optomechanical systems near their ground state has been reported [1–4], with demonstrations of a number of quantum mechanical effects for mesoscopic systems [5–8], including the observation of entanglement of a microwave field with a mechanical oscillator, in an elegant electromechanical experiment [9]. This was predicted theoretically [10–12] and involves pulsed inputs [12,13].

The next outstanding goal is to observe the *nonlocal quantum correlations* known as EPR steering, as predicted by Einstein, Podolsky, and Rosen in their famous EPR paradox [14–16], for mesoscopic massive objects. Such a realization would be a precursor to experiments that directly probe the macroscopic reality of an object [17,18]. It is of fundamental interest not only whether an optical field can entangle with a massive oscillator but also whether the two systems can show these strange directional “spooky action-at-a-distance” [19] effects that Schrödinger called “steering” [20–22].

Here we carry out a scalable, probabilistic quantum simulation of the standard nonlinear optomechanical model, in a regime allowing entanglement and EPR steering of the mechanical oscillator. This fully elucidates the quantum mechanical interplay between entanglement generation and thermal decoherence. We study the dynamical generation of correlations between the oscillator and an output pulse for realistic parameters. In our simulations we utilize the exact positive- P ($+P$) phase-space method [23], which has a positive probability distribution for all quantum states. Our work passes the barrier set by Olsen *et al.* for their pendular cavity quantum simulation [24]. This used the $+P$ method but with a different noise model, and with high temperatures that do not allow entanglement. Other earlier optomechanical calculations make assumptions ranging from linearization [10] to adiabatic approximations [12], or both.

A limitation in current optomechanics experiments is that long interaction times lead to increased decoherence, owing to a coupling to the environment at relatively high temperature.

It was recently proposed that this could be overcome by creating and verifying entanglement with pulses of light on fast time scales [12,13]. This was an adiabatic, linearized study [25]. The authors showed that entanglement is feasible, provided $Qf \gg k_m T_{\text{bath}}/h$, where T_{bath} is the temperature of the environment, f is the frequency of mechanical oscillator, and Q is the cavity quality. By comparison, we can treat arbitrary pulse shapes, the method is exact rather than linearized, and we use optimized entanglement and EPR measures. We also compare our results with the truncated Wigner (tW) method [26], valid for large photon-numbers [27]. Both methods agree with the recent entanglement observations at JILA [9].

The $+P$ technique, used in other parametric simulations [28,29], has no approximations apart from those of the standard model [30]. It gives accurate results for realistic experimental parameters. Compared to direct diagonalization [31] or quantum trajectory approaches [32], the method readily scales to large Hilbert spaces [33] and is especially useful for low-order correlations [34]. Neither approximations [35] nor new hardware [36] are required. Such methods have potential for treating a new class of multimode optomechanical devices [37]. This allows a quantitative understanding of the validity of previous methods and predictions of new effects.

Our results validate some earlier predictions for the simplified model in Refs. [12,38]. They are useful for addressing EPR-steering experiments in optomechanics. While entanglement of pulse and oscillator is robust, without requiring a low-temperature reservoir, thermal noise can prevent steering of the mechanical system when it is thermally excited. This is a fundamentally asymmetric manifestation of nonlocality [38,39], beautifully illustrated by the oscillator-pulse system.

The paper is organized as follows. Section II gives our model and simulation equations. Section III presents approximate analytic results, and Sec. IV summarizes the entanglement and EPR-steering criteria. Section V presents our exact quantum simulation results, with Sec. VI giving the conclusions.

II. HAMILTONIAN AND OPERATOR EQUATIONS

We consider a single-mode optomechanical Fabry-Perot cavity with coherent pumping and damping. A diagram is

^{*}pdrummond@swin.edu.au

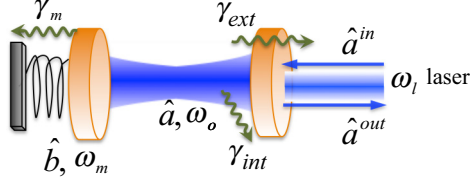


FIG. 1. (Color online) Two light pulses enter the cavity and interact with the mirror via radiation pressure. A first blue-detuned pulse entangles, while a second red-detuned pulse gives a readout.

shown in Fig. 1. We treat the regime of low temperatures and low mechanical damping, where quantum effects are observable. To generate entanglement and EPR steering, a blue-detuned pulse is used to entangle the mechanical oscillator with the output field. To verify entanglement, a second red-detuned pulse is coupled to the cavity-oscillator system to give a readout of the mechanical oscillator position.

A. Optomechanical Hamiltonian

The standard, single-mode optomechanical model is used [30,40]. The Hamiltonian includes the energy of the mechanical oscillator mode at ω_m , an input at ω_l , and the optical mode energy at angular frequency $\omega_o = \omega_l + \delta$. We transform to an interaction picture in which the time evolution of the cavity operators at the laser frequency is removed. This subtracts the term $\omega_l \hat{a}^\dagger \hat{a}$, together with corresponding time dependences, leaving

$$\begin{aligned} \hat{H}/\hbar = & \delta \hat{a}^\dagger \hat{a} + \omega_m \hat{b}^\dagger \hat{b} + \chi \hat{a}^\dagger \hat{a} (\hat{b} + \hat{b}^\dagger) \\ & + iE(t)(\hat{a}^\dagger - \hat{a}) + \hat{H}_r. \end{aligned} \quad (2.1)$$

The first terms give the energy of the optical cavity field and the mechanical oscillator, while the third term is the optomechanical interaction, where χ is the coupling due to radiation pressure. The fourth term is the coupling to the coherent input $E(t)$, and \hat{H}_r describes the coupling to dissipative reservoirs.

We define $k = [b, r] \equiv [\text{blue}, \text{red}]$ for the entangling and readout pulses, respectively. Following the strategy employed in Ref. [9], we first model the input of a blue-detuned laser pulse of duration τ . Thus, the cavity is initially resonant with the lower (Stokes) sideband of the input so that $\omega_o = \omega_l + \delta_b$, where $\delta_b = -\omega_m$. This enhances nonlinear generation of entanglement between a reflected output mode \hat{A}_b^{out} and the fundamental mode of the mechanical oscillator \hat{b} . We have simulated the correlations induced between the entangling pulse and the mechanical oscillator during this process.

After a short delay time τ_{del} , a red-detuned pulse of duration τ with the opposite detuning $\delta_r = \omega_m$ is input, transferring the mechanical oscillator state to the corresponding output field \hat{A}_r^{out} [12] as described below. The laser driving strength for the k th input pulse is $E(t) = E_0 \varepsilon(t) = \sqrt{2\gamma_o N_k} \varepsilon(t)$. Here N_k is the pulse photon number, and each envelope function $\varepsilon(t)$ is normalized so that $\int_{\tau_k^0}^{\tau_k^1} dt |\varepsilon(t)|^2 = 1$, where τ_k^0 and τ_k^1 are the start and end times of the k th pulse.

B. Master equation

This is a driven open system, and hence the density matrix must be calculated as the solution of a master equation. The master equation for the reduced density operator is valid [41] for regimes of Markovian behavior and weak damping, so that for $\gamma_j \ll \omega_j$

$$\begin{aligned} \frac{d\hat{\rho}}{dt} = & -\frac{i}{\hbar} [H, \hat{\rho}] + \sum_j \gamma_j \bar{n}_j (2\hat{a}_j^\dagger \hat{\rho} \hat{a}_j - \hat{a}_j \hat{a}_j^\dagger \hat{\rho} - \hat{\rho} \hat{a}_j \hat{a}_j^\dagger) \\ & + \sum_j \gamma_j (\bar{n}_j + 1) (2\hat{a}_j \hat{\rho} \hat{a}_j^\dagger - \hat{a}_j^\dagger \hat{a}_j \hat{\rho} - \hat{\rho} \hat{a}_j^\dagger \hat{a}_j). \end{aligned} \quad (2.2)$$

Here γ_o and γ_m are the optical decay rate and mechanical dissipation rate, while \bar{n}_j are the reservoir thermal occupations. Also, $\hat{\mathbf{a}} = (\hat{a}_1, \hat{a}_2) = (\hat{a}, \hat{b})$, with $j = 1, 2 \sim o, m$ indexing the optical and mechanical modes respectively.

There are often several distinct types of dissipation in experiments. Here we introduce two types of cavity loss, $\gamma_o = \gamma_{\text{ext}} + \gamma_{\text{int}}$, where γ_{ext} represents the output coupling through the mirrors to external propagating modes, while γ_{int} represents all other types of cavity losses. This distinction is necessary since only the part of the cavity loss that is externally coupled can result in operationally measurable entanglement. We note that Olsen *et al.* used a different, high-temperature master equation in their instructive simulations [24], which are for the strongly dissipative regime of low frequencies and high temperatures typical of gravity-wave detectors.

The master equation used here is equivalent to the following quantum Langevin equation:

$$\begin{aligned} \dot{\hat{a}} = & E(t) - (i\delta_k + \gamma_o) \hat{a} - i\chi \hat{a} (\hat{b} + \hat{b}^\dagger) + \sqrt{2\gamma_o} \hat{a}^{\text{in}}, \\ \dot{\hat{b}} = & -(i\omega_m + \gamma_m) \hat{b} - i\chi \hat{a}^\dagger \hat{a} + \sqrt{2\gamma_m} \hat{b}^{\text{in}}, \\ \dot{\hat{a}}^{\text{out}} = & \sqrt{2\gamma_{\text{ext}}} \hat{a} - \hat{a}_{\text{ext}}^{\text{in}}, \end{aligned} \quad (2.3)$$

where \hat{a}^{in} and \hat{b}^{in} are the input quantum noise amplitudes from the optical and mechanical reservoirs. Here \hat{a}^{out} describes the cavity output field mode, using standard input-output theory [42], and $\langle \hat{a}^{\text{out}\dagger}(t) \hat{a}^{\text{out}}(t) \rangle = \bar{\Phi}^{\text{out}}$ is the mean output flux in photons per second. The input-output relations involve only *external* damping and noise, which leads to an output coupling efficiency, $\eta_o = \gamma_{\text{ext}}/\gamma_o$. There are two different quantum Langevin terms, since while \hat{a}^{in} is coupled to the internal dynamics, there is also an orthogonal noise term $\hat{a}_\perp^{\text{in}}$ that only couples to the output, as in a beam splitter:

$$\begin{aligned} \hat{a}^{\text{in}} = & \sqrt{1 - \eta_o} \hat{a}_{\text{int}}^{\text{in}} + \sqrt{\eta_o} \hat{a}_{\text{ext}}^{\text{in}}, \\ \hat{a}_\perp^{\text{in}} = & \sqrt{\eta_o} \hat{a}_{\text{int}}^{\text{in}} - \sqrt{1 - \eta_o} \hat{a}_{\text{ext}}^{\text{in}}. \end{aligned} \quad (2.4)$$

The input reservoirs are assumed thermal and have correlations given approximately in the Markovian or wide-band noise limit by ideal noise sources with

$$\begin{aligned} \langle \hat{a}_i^{\text{in}\dagger}(t) \hat{a}_j^{\text{in}}(t') \rangle = & \bar{n}_{i,\text{th}} \delta_{ij} \delta(t - t'), \\ \langle \hat{a}_i^{\text{in}}(t) \hat{a}_j^{\text{in}\dagger}(t') \rangle = & [1 + \bar{n}_{i,\text{th}}] \delta_{ij} \delta(t - t'). \end{aligned} \quad (2.5)$$

To study output field correlations, we use a temporal mode decomposition to generate single-mode output operators with

bosonic commutation relations. These are

$$\hat{A}_k^{\text{in}} = \int_0^{\tau_m} dt u_k^{\text{in}}(t) \hat{a}^{\text{in}}(t), \quad (2.6)$$

with similar output mode definitions having in \rightarrow out. Here τ_m is the maximum interaction time, and the temporal input and output modes $u_k(t)$ have the normalization

$$\int_0^{\tau_m} dt u_k^*(t) u_j(t) = \delta_{kj}. \quad (2.7)$$

These operators commute with each other, apart from the bosonic commutation relations within the same mode. They also commute with system operators at *later* times, such as the mechanical oscillator position \hat{b} after an entanglement experiment [42].

However, both the quantum Langevin equations and the master equation are intractable without approximations, due to the large size of the Hilbert space combined with the nonlinear terms in the operator equations.

C. Phase-space equations

We now introduce an exact quantum simulation method that allows us to calculate dynamical behavior without approximations. This will be used to predict entanglement and EPR steering. As described elsewhere [23], we use standard operator identities in both normally ordered and symmetrically ordered phase-space distributions to transcribe the master equation (2.2) into c -number probabilistic phase space equations. These have features similar to phonon-photon coupling equations found in optical fiber simulations [27], as well as in earlier parametric oscillator simulations [28,29].

These methods allow dynamical quantum simulations of any optomechanical experiment of this type and can readily be generalized to many modes. As an example, in the following sections we analyze pulsed entanglement experiments where the entanglement between the mechanical oscillator and the first (blue-detuned) pulse is generated by the nonlinear interactions of the first pulse. The mechanical oscillator position is read out by the second pulse. This entanglement is then verified by measurements made on the first and second pulses.

1. Positive- P representation

First we use the positive- P representation [23], which gives a positive phase-space representation for *any* quantum state. This method uses a dimension-doubling approach in order to obtain a probabilistic distribution with a positive-definite diffusion. The transformation requires an assumption of vanishing boundary terms for the phase-space distribution [43]. Such terms are exponentially small for realistic open system parameter values, which we have verified from the low variances of our numerical results.

There are six independent complex phase-space variables $(\alpha, \alpha^+, \beta, \beta^+, \alpha^{\text{out}}, \alpha^{\text{out}+})$ for the cavity mode, the oscillator mode, and the output mode. These represent the operators $(\hat{a}, \hat{a}^\dagger, \hat{b}, \hat{b}^\dagger, \hat{a}^{\text{out}}, \hat{a}^{\text{out}\dagger})$ respectively via a normally ordered correspondence, with $\langle \alpha^+ \alpha \rangle_S = \langle \hat{a}^\dagger \hat{a} \rangle$, $\langle \beta^+ \beta \rangle_S = \langle \hat{b}^\dagger \hat{b} \rangle$, where $\langle \cdot \rangle_S$ is a stochastic and $\langle \cdot \rangle$ is a quantum average. After deriving the Fokker-Planck equation [44], one obtains an equivalent set

of complex Itô stochastic equations:

$$\begin{aligned} d\alpha &= \{E(t) - [i\delta_k + i\chi(\beta + \beta^+) + \gamma_o]\alpha\}dt + dW_1, \\ d\beta &= [-(i\omega_m + \gamma_m)\beta - i\chi\alpha\alpha^+]dt + dW_2, \\ d\alpha^+ &= \{E^*(t) + [i\delta_k + i\chi(\beta + \beta^+) - \gamma_o]\alpha^+\}dt + dW_1^+, \\ d\beta^+ &= [(i\omega_m - \gamma_m)\beta^+ + i\chi\alpha\alpha^+]dt + dW_2^+, \\ d\alpha^{\text{out}} &= \sqrt{2\gamma_{\text{ext}}}\alpha - d\alpha_{\text{ext}}^{\text{in}}, \\ d\alpha^{\text{out}+} &= \sqrt{2\gamma_{\text{ext}}}\alpha^+ - d\alpha_{\text{ext}}^{\text{in}+}. \end{aligned} \quad (2.8)$$

The Gaussian noises dW_i are due to both internal nonlinearities and thermal noise inputs, so that $dW_i = dW_i^x + dW_i^{\text{th}}$, where

$$\begin{aligned} dW_1^{\text{th}} &= \sqrt{2\gamma_{\text{int}}}\alpha_{\text{int}}^{\text{in}} + \sqrt{2\gamma_{\text{ext}}}\alpha_{\text{ext}}^{\text{in}}, \\ dW_2^{\text{th}} &= \sqrt{2\gamma_m}\beta^{\text{in}}. \end{aligned} \quad (2.9)$$

Here we need to treat the two types of cavity noise separately. In all cases the nonvanishing stochastic thermal correlations are

$$\langle d\alpha_k^{\text{in}} d\alpha_l^{\text{in}+} \rangle_S = \bar{n}_{k,\text{th}} \delta_{kl} dt, \quad (2.10)$$

where $k, l = 0, 1, 2 \sim \text{int, ext, } m$, and $\bar{n}_{k,\text{th}}$ are the mean heat bath occupations. Here we use the notation $d\alpha_m^{\text{in}} \equiv d\beta^{\text{in}}$. In addition, the positive- P method includes quantum noise due to interactions, with correlations

$$\begin{aligned} \langle dW_i^x dW_j^x \rangle_S &= -i\delta_{i,3-j}\chi\alpha dt, \\ \langle dW_i^{x+} dW_j^{x+} \rangle_S &= i\delta_{i,3-j}\chi\alpha^+ dt. \end{aligned} \quad (2.11)$$

Input-output mode c -number representations are defined in a similar way to the corresponding operator quantities, as

$$A_k^{\text{in}} = \int_0^{\tau_m} dt u_k^{\text{in}}(t) \alpha^{\text{in}}(t). \quad (2.12)$$

The equations have analytic solutions via stochastic diagram methods [45] and also allow exact probabilistic quantum simulations via an ensemble of trajectories, which can be integrated numerically [46].

2. Wigner representation

Another approach that is simpler—but approximate—is the truncated Wigner distribution [26], which is a symmetrically ordered representation. Here there are three independent complex phase-space variables $(\alpha, \beta, \alpha^{\text{out}})$. These represent the operators via asymmetrically ordered correspondence, with $\langle \alpha^* \alpha \rangle_S = \langle \hat{a}^\dagger \hat{a} + 1/2 \rangle$, $\langle \beta^* \beta \rangle_S = \langle \hat{b}^\dagger \hat{b} + 1/2 \rangle$. After truncating derivatives higher than second order in the Fokker-Planck equation (valid at large photon number), we obtain

$$\begin{aligned} d\alpha &= \{E(t) - [i\delta_k + i\chi(\beta + \beta^*) + \gamma_o]\alpha\}dt + dW_1^{\text{th}}, \\ d\beta &= [-(i\omega_m + \gamma_m)\beta - i\chi|\alpha|^2]dt + dW_2^{\text{th}}, \\ d\alpha^{\text{out}} &= \sqrt{2\gamma_{\text{ext}}}\alpha - d\alpha_{\text{ext}}^{\text{in}}. \end{aligned} \quad (2.13)$$

Here the thermal Gaussian noise correlations are as given in Eq (2.9), except that they now correspond to symmetric ordering of the reservoir operators, with correlations

$$\langle d\alpha_i^{\text{in}} d\alpha_j^{\text{in}*} \rangle_S = (\bar{n}_{i,\text{th}} + 1/2) \delta_{ij} dt. \quad (2.14)$$

Input-output mode c -number representations are defined as in Eq (2.12). The stochastic correlations for these quantities are equivalent to symmetrically ordered operator products. These equations also imply that $\langle |\alpha|^2 \rangle_S = \langle \hat{n} + 1/2 \rangle = 1/2$ when there is no driving or coupling. Although approximate, this method is simple. It provides a rigorous justification for the methods used to analyze recent electromechanics experiments [9], but has fewer restrictions than this adiabatic approach.

III. ADIABATIC LINEARIZED MODEL

In the special case of linearized, adiabatic pulses, Hofer *et al.* [12] have shown how to describe optomechanical entanglement using an approximate Hamiltonian. In this subsection we review their approach. It is useful to start with an adiabatic Hamiltonian [10] that illustrates the physics. This approximation is not used in the exact simulations described later, but it demonstrates the source of the entanglement and read-out couplings.

A. Adiabatic Hamiltonian

In the adiabatic limit of large detuning, the mean intracavity field is dominated by external driving and damping, so that

$$\langle \hat{a} \rangle \approx E(t) - (i\delta_k + \gamma_o) \langle \hat{a} \rangle, \quad (3.1)$$

which has the steady-state solution

$$\langle \hat{a} \rangle = \bar{\alpha}_k \approx \frac{E}{i\delta_k + \gamma_o}. \quad (3.2)$$

We now examine the small fluctuations around the steady state, by introducing $\delta\hat{a} = \hat{a} - \langle \hat{a} \rangle$. The derivation of this transformation is well known [10,12]. Expanding the Hamiltonian to first order in the interactions of these small fluctuations, and defining the adiabatic coupling $g_{k,a} = i\chi\bar{\alpha}_k$, gives the adiabatic interaction Hamiltonian at large detunings:

$$\hat{H}_a/\hbar \approx i(g_{k,a}^* \delta\hat{a} - g_{k,a} \delta\hat{a}^\dagger)(\hat{b} + \hat{b}^\dagger). \quad (3.3)$$

Next, it is convenient to use operators in a frame rotating with δ_k , defined as $\hat{a}^r \equiv \delta\hat{a}e^{i\delta_k t}$, $\hat{b}^r = \hat{b}e^{i\omega_m t}$, and employ the rotating-wave approximation to focus on quasiresonant terms. There are two limits of interest here:

(1) Blue-detuned

First, consider the blue-detuned case of $\delta_b = -\omega_m$, with $|\delta_b| \gg \gamma_o$. The resonant interaction terms are given by the squeezing and entanglement Hamiltonian:

$$\hat{H}_a/\hbar = i(g_{k,a}^* \hat{a}^r \hat{b}^r - g_{k,a} \hat{a}^{r\dagger} \hat{b}^{r\dagger}). \quad (3.4)$$

(2) Red-detuned

In the red-detuned case of $\delta_b = \omega_m$, the resonant interaction terms are given by the beam-splitter Hamiltonian:

$$\hat{H}_a/\hbar = i(g_{k,a}^* \hat{a}^r \hat{b}^{r\dagger} - g_{k,a} \hat{a}^{r\dagger} \hat{b}^r). \quad (3.5)$$

A normalized output mode in the rotating frame is obtained using the standard cavity input-output relations [42] given in Eq (2.3), together with a mode function designed to match the gain characteristics of the cavity [12]. To achieve this, define

input-output mode functions as

$$u_k^{\text{in}}(t) = \sqrt{\frac{1}{\mathcal{N}_k(\tau)}} e^{i\delta_k t \pm R_k^{\text{in}}(t)}, \quad (3.6)$$

where $R_k^{\text{in}}(t) = \int_0^t G_k^{\text{in}}(t') dt'$ and the normalization is $\mathcal{N}_k^{\text{in}}(\tau) = \int_{\tau_k^0}^{\tau_k^{\tau}} e^{2R_k^{\text{in}}(t)} dt$. There are similar expressions with $in \rightarrow out$, making four modes in all. The optomechanical gain is $G_k(t) = \pm |g_{k,a}|^2 / \gamma_o = \pm \chi^2 E(t)^2 / \gamma_o (\delta_k^2 + \gamma_o^2)$. For output modes there is a positive sign for the first (blue-detuned) pulse and negative for the second (red-detuned) pulse. These signs are reversed for the input modes. Since we only are interested in fluctuations, we consistently drop the mean value part of the input-output mode operators.

There is a characteristic phase of $e^{i\phi_b} = -g_{b,a}/|g_{b,a}|$ for entanglement and $e^{i\phi_r} = g_{r,a}/|g_{r,a}|$ for readout, where from Eq. (3.2), we see that $\phi_k = \tan^{-1}(\gamma_o/\delta_k)$ in both cases. This means that the phases for entanglement and readout have equal magnitudes and opposite signs.

B. Linearized entanglement generation

In the ideal linearized model, including an adiabatic approximation, the Heisenberg equations resulting from considering only the squeezing or entanglement Hamiltonian, Eq. (3.4), are

$$\begin{aligned} \dot{\hat{a}}^r &= -\gamma_o \hat{a}^r - g_{b,a} \hat{b}^{r\dagger} + \sqrt{2\gamma_o} \hat{a}^{r,\text{in}}, \\ \dot{\hat{b}}^r &= -g_{b,a} \hat{a}^{r\dagger}. \end{aligned} \quad (3.7)$$

This has an adiabatic solution, provided $\gamma_o \tau \gg 1$:

$$\hat{a}^r = -\frac{g_{b,a}}{\gamma_o} \hat{b}^{r\dagger} + \sqrt{\frac{2}{\gamma_o}} \hat{a}^{r,\text{in}}, \quad (3.8)$$

$$\hat{b}^r = e^{Gt} \hat{b}^r(0) - g_{b,a} \sqrt{\frac{2}{\gamma_o}} e^{Gt} \int_0^\tau ds e^{-Gs} \hat{a}^{r,\text{in}}(s),$$

where we have defined $G = G_b^{\text{out}} = |g_{b,a}|^2 / \gamma_o$ as the blue-detuned entanglement gain.

In the rotating frame, with rectangular-shaped pulses and temporal light modes defined in Eq. (3.6), we obtain

$$\begin{aligned} \hat{A}^{\text{in}} &= \sqrt{\frac{2G}{1 - e^{-2G\tau}}} \int_0^\tau dt e^{-Gt} \hat{a}^{r,\text{in}}(t), \\ \hat{A}_\perp^{\text{in}} &= \sqrt{\frac{2G}{e^{2G\tau} - 1}} \int_0^\tau dt e^{Gt} \hat{a}_\perp^{r,\text{in}}(t), \\ \hat{A}^{\text{out}} &= \sqrt{\frac{2G}{e^{2G\tau} - 1}} \int_0^\tau dt e^{Gt} \hat{a}^{r,\text{out}}(t). \end{aligned} \quad (3.9)$$

This leads to the input-output relations

$$\begin{aligned} \hat{A}^{\text{out}} &= \sqrt{\eta_0} [e^{G\tau} \hat{A}^{\text{in}} + e^{i\phi_b} \sqrt{e^{2G\tau} - 1} \hat{B}^{\text{in}\dagger}] + \sqrt{1 - \eta_0} \hat{A}_\perp^{\text{in}}, \\ \hat{B}^{\text{out}} &= e^{G\tau} \hat{B}^{\text{in}} + e^{i\phi_b} \sqrt{e^{2G\tau} - 1} \hat{A}^{\text{in}\dagger}, \end{aligned} \quad (3.10)$$

where $\hat{B}^{\text{in}} \equiv \hat{b}^r(0)$ and $\hat{B}^{\text{out}} \equiv \hat{b}^r(\tau)$. If $\eta_0 = 1$, then in the limit of $R = G\tau \gg 1$, we get the relations $\hat{A}^{\text{out}} = e^R (\hat{A}^{\text{in}} + e^{i\phi_b} \hat{B}^{\text{in}\dagger})$, $\hat{B}^{\text{out}} = e^R (\hat{B}^{\text{in}} + e^{i\phi_b} \hat{A}^{\text{in}\dagger})$.

C. Linearized readout procedure

Analogously to the calculation above, but using the beam-splitter interaction Hamiltonian (3.5), one obtains the Heisenberg equations for the red-detuned case:

$$\begin{aligned}\dot{\hat{a}}^r &= -\gamma_o \hat{a}^r - g_{r,a} \hat{b}^{r\dagger} + \sqrt{2\gamma_o} \hat{a}^{r,\text{in}}, \\ \dot{\hat{b}}^r &= g_{r,a}^* \hat{b}^r.\end{aligned}\quad (3.11)$$

Introducing the readout gain, $G' = G_r^{\text{out}} = |g_{r,a}|^2/\gamma_o$, gives the adiabatic solution

$$\begin{aligned}\hat{a}^r &= -\frac{g_{r,a}}{\gamma_o} \hat{b}^r + \sqrt{\frac{2}{\gamma_o}} \hat{a}^{r,\text{in}}, \\ \hat{b}^r &= e^{-G't} \hat{b}^r(0) - g_{r,a}^* \sqrt{\frac{2}{\gamma_o}} e^{-G't} \int_0^t ds e^{G's} \hat{a}^{r,\text{in}}(s).\end{aligned}\quad (3.12)$$

The temporal light modes of Eq. (3.6) now become

$$\begin{aligned}\hat{A}_r^{\text{in}} &= \sqrt{\frac{2G'}{e^{2G'\tau} - 1}} \int_{\tau_0'}^{\tau+\tau_0'} e^{G't} \hat{a}^{r,\text{in}} dt, \\ \hat{A}_\perp^{\text{in}} &= \sqrt{\frac{2G'}{1 - e^{-2G'\tau}}} \int_{\tau_0'}^{\tau+\tau_0'} dt e^{-G't} \hat{a}_\perp^{r,\text{in}}(t), \\ \hat{A}_r^{\text{out}} &= \sqrt{\frac{2G'}{1 - e^{-2G'\tau}}} \int_{\tau_0'}^{\tau+\tau_0'} e^{-G't} \hat{a}^{r,\text{out}} dt.\end{aligned}\quad (3.13)$$

This results in the input-output relation

$$\begin{aligned}\hat{A}_r^{\text{out}} &= \sqrt{\eta_o} [-e^{i\phi_r} \sqrt{\eta_o(1 - e^{-2G'\tau})} \hat{B}_r^{\text{in}} + e^{-G'\tau} \hat{A}_r^{\text{in}}] \\ &\quad + \sqrt{1 - \eta_o} \hat{A}_{\perp r}^{\text{in}},\end{aligned}\quad (3.14)$$

where $\hat{B}_r^{\text{in}} \equiv \hat{B}^{\text{out}}$ gives the initial operator for the mechanical oscillator, which is now entangled by the previous interaction, and \hat{A}_r^{out} and \hat{A}_r^{in} give the output and input red-detuned pulses. The coupling is such that in the large gain limit $R' \equiv G'\tau \gg 1$, with $\eta_o = 1$, the red-detuned output pulse \hat{A}_r^{out} gives a readout of the initial amplitude \hat{B}_r^{in} of the mechanical oscillator after entanglement.

This is an idealized picture which helps to explain intuitively why these experiments can be regarded as quantum measurements of the oscillator position. In the quantum simulations carried out here, we include a full multimode analysis of all output fields, including losses and without adiabatic or single-mode approximations.

IV. ENTANGLEMENT AND EPR-STEERING MEASURES

To signify entanglement and EPR steering, it is convenient to consider quadrature measurements. The entangling and readout pulse output field quadratures are given by

$$\hat{X}_k^\theta = \frac{1}{2}[e^{-i\theta} \hat{A}_k(\tau) + e^{i\theta} \hat{A}_k^\dagger(\tau)], \quad (4.1)$$

respectively. We denote $\hat{P}_k^\theta = \hat{X}_k^{\theta+\pi/2}$, with the angle dropped when $\theta = 0$. We see from the previous section that for large gain $\hat{A}_r^{\text{out}} \rightarrow -e^{i\phi_r} \hat{B}_r^{\text{in}}$. For the full entanglement protocol, consisting of a blue-detuned entanglement pulse followed by a red-detuned readout pulse, in the limit $R \gg 1$ as well as $R' \gg 1$, this yields $\hat{X}_b + \hat{X}_r^{\phi_b+\phi_r} \rightarrow 0$ and $\hat{P}_b - \hat{P}_r^{\phi_b+\phi_r} \rightarrow 0$, where

\hat{X}_b (\hat{P}_b) and \hat{X}_r (\hat{P}_r) mean the quadratures corresponding to the output field of the first (blue-detuned) and the second (red-detuned) pulse, respectively. Hence, the final quadrature of the mechanical oscillator

$$\hat{X}_m^\varphi(\tau) = \frac{1}{2}[e^{-i\varphi} \hat{b}^r(\tau) + e^{i\varphi} \hat{b}^{r\dagger}(\tau)] \quad (4.2)$$

is transferred to the red-detuned output pulse quadrature, \hat{X}_r^θ , with a sign change.

This leads to measurable entanglement and EPR correlations between the red- and blue-detuned output field quadratures. In the numerical calculations, we optimize the phase choice θ for best entanglement, as is also done experimentally. We calculate both the correlations of the mechanical oscillator with the entangling blue-detuned pulse, and also the correlations between the two outputs, as measured in current experiments.

A. Entanglement measures

We next consider how to signify entanglement between the reflected entangling field \hat{X}_b^θ and either the mechanical quadrature \hat{X}_m^θ or the readout pulse \hat{X}_r^θ . For clarity, we generally write \hat{X}_m^θ in the following criteria, although we also simulate results with a readout pulse \hat{X}_r^θ , as measured in current experiments. There are numerous possible entanglement measures.

1. Product criteria

The most robust measures are the *product* signatures first introduced for EPR steering [15] and applied to entanglement by Tan [47]. The most general inequalities of this type include a measurement gain g . Entanglement is verified if [38,48]

$$\Delta_{\text{ent}}^p = \frac{4\Delta(\hat{X}_m - g\hat{X}_b^\theta)\Delta(\hat{P}_m + g\hat{P}_b^\theta)}{(1 + g^2)} < 1, \quad (4.3)$$

where we introduce the notation $(\Delta\hat{x})^2 \equiv \langle \hat{x}^2 \rangle - \langle \hat{x} \rangle^2$, $\langle \hat{x}, \hat{y} \rangle = \langle \hat{x}\hat{y} \rangle - \langle \hat{x} \rangle \langle \hat{y} \rangle$, and take $\varphi = 0$. Here g represents real gains used in postprocessing the data. The gain g and phase θ is optimized numerically in some of our simulations, but not all, to show the effect of the optimization.

We assume for simplicity the same gain value for both variances. For example, if we only optimize the gain, then from minimizing Δ_{ent}^p , one obtains

$$g = \frac{1}{2a}[-b + \sqrt{b^2 - 4ac}], \quad (4.4)$$

where $c = \langle \hat{X}_m, \hat{X}_b \rangle = -a$ and $b = (\Delta\hat{X}_b)^2 - (\Delta\hat{X}_m)^2$.

For dealing with the red-detuned readout pulse, we replace \hat{X}_m by $-\hat{X}_r$, and \hat{P}_m by $-\hat{P}_r$, as motivated in the previous section, giving the criterion

$$\Delta_{\text{ent}}^p = \frac{\Delta(\hat{X}_r + g\hat{X}_b^\theta)\Delta(\hat{P}_r - g\hat{P}_b^\theta)}{(1 + g^2)/4} < 1. \quad (4.5)$$

2. Additive criteria

A weaker *additive* criterion can be obtained from this, which is

$$\Delta_{\text{ent}}^a = \frac{\Delta^2(\hat{X}_m - g\hat{X}_b) + \Delta^2(\hat{P}_m + g\hat{P}_b)}{(1 + g^2)/2} < 1, \quad (4.6)$$

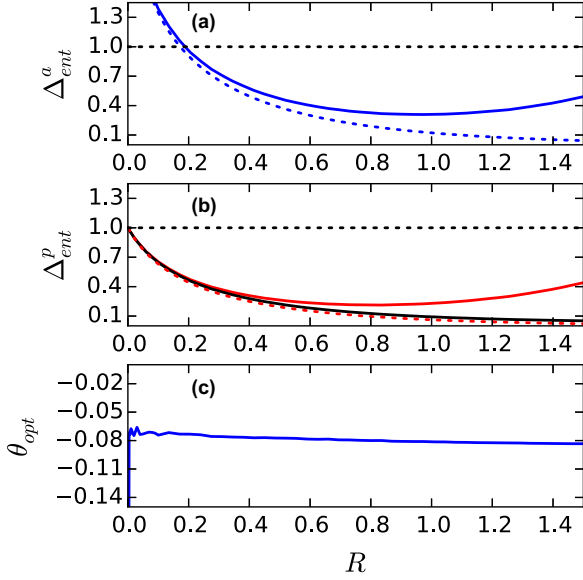


FIG. 2. (Color online) Various entanglement signatures are plotted vs R . Plots (a), (b), and (c) show the simulation results and approximate adiabatic predictions for the optomechanical experiment described in Sec. VB, with an initial and heat bath temperature of $T = 500$ mK. Plot (a) shows the additive criterion Δ_{ent}^a where the gain factor is fixed at $g = 1$, with the solid line representing the simulation results and the dotted line the adiabatic prediction. Plot (b) shows the product criterion Δ_{ent}^p where the gain factor g is chosen optimally to minimize Δ_{ent}^p , but the relative phase is fixed at $\theta = 0$. Here again the solid line represents the simulation results and the dotted line the approximate adiabatic prediction. The black curve shows the simulation result for the product criterion Δ_{ent}^p , where both g and θ are chosen optimally. Plot (c) shows the optimal phase angle θ that corresponds to the black curve.

where g can again be chosen optimally. The choice $g = 1$ is not always optimal but leads to one of the most widely used entanglement criteria [25]:

$$\Delta_{\text{ent}}^a = [\Delta(\hat{X}_m - \hat{X}_b)]^2 + [\Delta(\hat{P}_m + \hat{P}_b)]^2 < 1. \quad (4.7)$$

The difference is that $\Delta_{\text{ent}}^p < 1$ is a more robust entanglement signature. This detects entanglement that the weaker criterion of $\Delta_{\text{ent}}^a < 1$ is unable to detect. As described above, for dealing with the red-detuned readout pulse, we replace \hat{X}_m by $-\hat{X}_r$, and \hat{P}_m by $-\hat{P}_r$. We use the more robust product signatures in our numerical results, except for comparison to electromechanical experiments where the additive criterion with $g = 1$ was used to process the data.

Using the input-output relations of the linearized adiabatic model, one obtains after some algebra a theoretical adiabatic prediction for Eq. (4.7) of

$$\Delta_{\text{ent,ad}}^a = (\bar{n}_{b,0} + 1)(e^R - \sqrt{e^{2R} - 1})^2. \quad (4.8)$$

However, this simplified picture neglects inefficiencies, as well as the thermal noise added to the mechanical oscillator as it interacts with its thermal reservoir.

3. Comparisons of entanglement criteria

Figure 2 shows a comparison of the product and additive entanglement criteria for the conditions of an optomechanical experiment described in Sec. VB, with a bath temperature chosen as $T = 500$ mK. One can see that the gain-optimized product criterion is more robust than the additive criterion where $g = 1$ has been fixed; that is, it is more sensitive to the presence of entanglement. This can be seen in both the adiabatic predictions and the full simulation results.

This graph also shows how the accuracy of the adiabatic model changes with pump strength. While there is good agreement between the simulation results for Δ_{ent}^a and Δ_{ent}^p and the adiabatic predictions for small values of R ; that is, for a small pump strength, the simulation results diverge from their theoretical predictions for higher pump strengths. The entanglement signatures begin to deteriorate from a value of $R \approx 1$ for Δ_{ent}^a and $R \approx 0.8$ for Δ_{ent}^p .

Surprisingly, the phase- and gain-optimized product criterion is in very good agreement with the adiabatic prediction for Δ_{ent}^p , even though the adiabatic prediction assumes that $\theta = \varphi = 0$, which in fact are not the optimal parameters.

The third subgraph of Fig. 2 shows the optimal phase angle that corresponds to the black curve. The phase shift of $\Delta\varphi \approx -0.075$ is as expected from the adiabatic prediction, as it is approximately equal to $-\gamma_o/\omega_m = -0.0703$.

B. EPR-steering criteria

The more demanding EPR-steering paradox is established through violation of the Reid-EPR inequality [15,16]. This tests whether an inferred Heisenberg uncertainty relation is violated under the assumptions of local realism (LR). The paradox is *directional*, so that one obtains different criteria depending on the direction of inference. If one infers the oscillator position from the blue readout, then the paradox occurs if

$$\begin{aligned} E_{m|b} &= 4\Delta_{\text{inf}}\hat{X}_m\Delta_{\text{inf}}\hat{P}_m \\ &= 4\Delta(\hat{X}_m - g\hat{X}_b^\theta)\Delta(\hat{P}_m + g\hat{P}_b^\theta) < 1. \end{aligned} \quad (4.9)$$

Here $\Delta_{\text{inf}}\hat{X}_m$, $\Delta_{\text{inf}}\hat{P}_m$ are the inferred uncertainties, and the optimal gain is given as $g = (\hat{X}_m, \hat{X}_b)/(\Delta\hat{X}_b)^2 = -(\hat{P}_m, \hat{P}_b)/(\Delta\hat{P}_b)^2$, owing to the symmetries of this problem. For a Reid-EPR paradox achieved by condition (4.9), measurements on the pulse system enable “steering” of the mechanical oscillator m [21,22]. This criterion with optimal g_x, g_p is necessary and sufficient for EPR steering in two-mode Gaussian systems [15,21].

A thermal barrier exists for this paradox. Figure 6 shows that the mechanical oscillator is steerable by the optical pulse system when $r > r_0$, where a minimum strength r_0 of the gain parameter required, for a given $n_{b,0}$. A thermal barrier means that a threshold level of pulse-oscillator interaction is required for a given thermal occupation $n_{b,0}$ of the oscillator.

An EPR paradox can be shown the other way, by the criterion

$$E_{b|m} = 4\Delta(\hat{X}_b - g\hat{X}_m^\phi)\Delta(\hat{P}_b + g\hat{P}_m^\phi) < 1. \quad (4.10)$$

We similarly modify the EPR-steering criteria when observing two correlated optical outputs, replacing \hat{X}_m by $-\hat{X}_r$, and \hat{P}_m by $-\hat{P}_r$.

V. QUANTUM SIMULATIONS

We assume the input state of both light fields and the mirror to be a thermal state with mean excitation number $\bar{n}_{k,0}$, so that $\Delta\hat{X}_k(0) = \Delta\hat{P}_k(0) = \sqrt{\bar{n}_{k,0}/2 + 1/4}$. Our quantum simulations fully model both the blue- and red-detuned pulses, without linearization or adiabatic assumptions. Plots of the results of our full simulations with the red-detuned output pulse are shown together with comparisons to idealized mechanical oscillator measurements.

A. Electromechanical experiment

In the pioneering electromechanical experiment carried out recently by Palomaki *et al.* [9], an inductor-capacitor (LC) resonator that interacts with an external microwave field was coupled to a mechanical oscillator. This corresponds to the usual optomechanical experiments, except with an LC resonator replacing the optical cavity and a microwave field replacing the laser driving field. We give our simulation results for this case first. The good agreement with experimental measurements verifies our quantum simulations. This also indicates some of the limitations of the experiment, due to noise and inefficiency issues.

1. Electromechanical parameters

We simulated the recent microwave experiment leading to quantum entanglement, using the published parameter values [9] and the reported quantum efficiency of $\eta = 0.2$. The electromechanical (microwave) experimental parameters are $\omega_m/2\pi = 10.34$ MHz for the mechanical oscillator frequency, $\chi_0/2\pi = 200$ Hz for the coupling constant between LC resonator and mechanical oscillator, $\gamma_{\text{int}}/2\pi = 30$ kHz for the internal LC resonator dissipation rate, $\gamma_{\text{ext}}/2\pi = 150$ kHz for the external LC resonator dissipation rate, $\gamma_m/2\pi = 17.5$ Hz for the mechanical oscillator dissipation rate, $\tau_b = \tau_r = 35.5$ μs for the pulse duration of both the blue- and red-detuned pulse, and $\tau_{\text{del}} = 10$ μs for the delay time between the two pulses. The experimental paper quoted intensity decay rates, while we consistently use amplitude decay rates to quantify dissipation.

In the electromechanical experiments, the mechanical oscillator was precooled so that the initial phonon occupation number was $\bar{n}_{m,0} = 0.5 \pm 0.1$. The LC resonator experienced excess technical noise, giving initial variances of $\bar{n}_{o,0} = 0.12 \pm 0.02$. During the time of the experiment, the mechanical oscillator was in contact with a heat bath at 19 mK, so that $\bar{n}_{m,\text{th}} = 37.8$. There was an initial wait period of 15 μs , during which time we calculate there was a preheating from the heat bath to an occupation number of $\bar{n}_{m,0} = 0.62 \pm 0.1$. An additional electromagnetic noise of $\bar{n}_{o,\text{th}} = 0.12 \pm 0.02$, the same as found initially, was present in both the internal and external input reservoirs of the LC resonator. This additional noise and corresponding relaxation makes for a substantial difference with the optomechanical situation. It is caused by the typically higher technical noises found with microwave sources, as compared with optical laser sources of radiation.

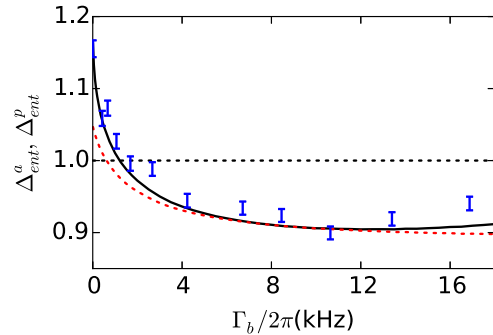


FIG. 3. (Color online) Predicted entanglement signatures vs pump strength Γ_b for the microwave experiment of Ref. [9], using their notation. The black curve gives the additive entanglement signature Δ_{ent}^a at $g = 1$. This shows good agreement with the experimental data and also excellent agreement with a linearized calculation in Ref. [9], except for small differences at large Γ_b . The circles are experimental values for Δ_{ent}^a . The red dotted line gives the result of the phase- and gain-optimized product signature, Δ_{ent}^p .

The quantum efficiency of the detector was experimentally measured as $\eta = 0.20 \pm 0.01$. The pump strength of the transfer pulse was fixed at $\Gamma_r/2\pi = 11$ kHz while the pump strength of the entanglement pulse was varied over a range of $\Gamma_b/2\pi = 0 \dots 18$ kHz. These pump strengths were defined as intensity gains or losses, so that in our notation $G_k = \pm\Gamma_k/2$.

2. Entanglement simulation results

The results of the simulations are compared to experiment in Fig. 3. This used an additive entanglement criterion with unit gain ($g = 1$), and a relative phase adjusted to optimize the correlations.

To simplify comparisons, we use the notation and entanglement signatures used in the experiment. The definition for the pump strength given in the experimental paper was

$$\Gamma_k = \frac{2\chi^2 \bar{n}_{k,\text{ind}}}{\gamma_o}, \quad (5.1)$$

where $\bar{n}_{k,\text{ind}}$ is the number of coherently induced photons in the cavity under adiabatic conditions, i.e.,

$$\bar{n}_{k,\text{ind}} = \langle |\alpha|^2 \rangle_\infty \approx \frac{E^2}{\delta^2 + \gamma_o^2}. \quad (5.2)$$

Using the relationship $E_k^2 \tau_k = 2\gamma_{\text{ext}} N_k$, which gives the pump amplitude E_k in terms of the total number of external pump photons N_k , we conclude that the experimental parameters Γ_r , Γ_b can be expressed in terms of the earlier definitions as

$$\Gamma_k = \frac{4\chi^2 \eta_o N_k}{(\omega_m^2 + \gamma_o^2) \tau_k}, \quad (5.3)$$

where $k = [r, b]$, and $\gamma_o = \gamma_{\text{ext}} + \gamma_{\text{int}}$ denotes the total dissipation rate for the LC resonator. For comparison purposes, our amplitude gain G_k is therefore given by

$$G_k = \pm\Gamma_k/2. \quad (5.4)$$

In summary, the figure gives a comparison of the exact simulations vs experimental results for electromechanical pulse entanglement at microwave frequencies. We obtain good

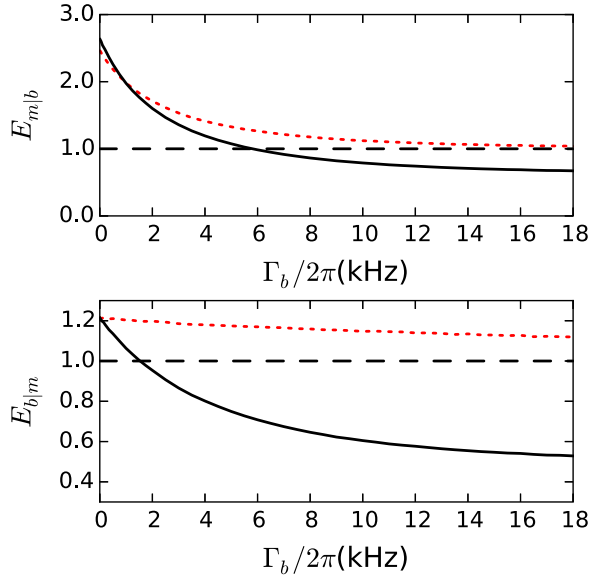


FIG. 4. (Color online) EPR steering versus entanglement pump strength Γ_b , for the electromechanical conditions used in Fig. 3, except with $\eta = 0.9$. Dashed lines indicate the result of using optical readouts; solid lines assume direct oscillator measurements. The predictions are for the electromechanical microwave experiment. Although we assume a higher efficiency, the upper curves show how the noisy readout process degrades EPR steering in the output fields. The lower curves assume a direct, low-noise readout of the oscillator position is obtained through some other technique.

agreement between the simulation and the experimental data of Palomaki *et al.* [9]. These results are also in agreement with linearized calculations [9], thus verifying that these approximations are valid. However, the exact simulations can also be used in nonlinear regimes where linearization will fail.

3. EPR-steering violations

It is known that EPR steering is not possible when the efficiency reduces below 0.5 for the steering (pulse) system [49]. As a result, the microwave experimental parameters are less favorable for EPR steering owing to low quantum efficiencies of $\eta \approx 0.2$. For this reason, we assume a higher efficiency of $\eta = 0.9$ in these EPR calculations. After all, detector efficiency is a moving target, and much higher efficiencies may occur in future.

Even with higher efficiency, however, our simulation reveals no steering for external measurements using the noise parameters of this experiment (inset of Fig. 4), due to the high input noise levels in the measuring pulse inputs. Experiments with lower input noise levels are necessary for EPR-steering observation.

B. Optomechanical experiment

In the optomechanical simulations, we choose typical parameters that correspond to recent optomechanical experiments. The highest temperatures we simulate are 4 K. This is lower than in some reported data, although this temperature appears to be in the currently accessible range. We calculate

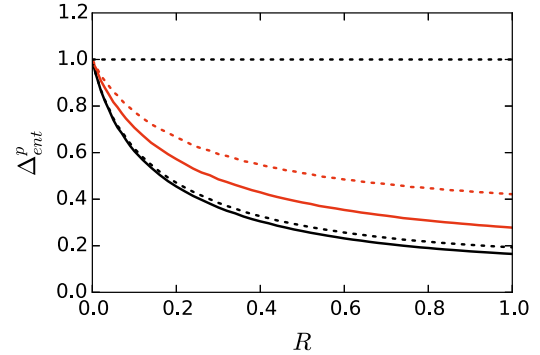


FIG. 5. (Color online) The entanglement signature Δ_{ent}^p is plotted vs R , for an initial mechanical occupation number $\bar{n}_{m,0} = 0.7$ and two values of heat bath occupation $\bar{n}_{m,th} = 0.7$ (lower), 22.1 (upper) for the oscillator corresponding to temperatures $T = 200$ mK and 4 K. The optical cavity bath is assumed a vacuum, i.e., $\bar{n}_{o,0} = \bar{n}_{o,th} = 0$. The solid lines give the oscillator entanglement; the dotted lines give results of the probe measurements.

the robust product entanglement measure Δ_{ent}^p , with optimal gain and phase.

1. Si optomechanical crystal structures

Parameters are reported in Ref. [2], with $\omega_m/2\pi = 3.7$ GHz, $Q_m = \omega_m/\gamma_m = 10^5$, $\gamma_m/2\pi = 37$ KHz, $\gamma_o/2\pi = 0.26$ GHz, and $\chi_o/2\pi = 910$ KHz. We choose the photon number for the red transfer pulse as $N_r = 24.6 \times 10^6$, corresponding to a readout gain of $R' = 3$, while for the first pulse a photon number up to $N_b = 8.2 \times 10^6$ is used, corresponding to an entanglement gain $R = 1$. Both pulses have a duration of $\tau = 0.04 \mu\text{s}$, and the delay time is set to $\tau_{del} = 0.008 \mu\text{s}$. We assumed $\gamma_{int} = 0$ —i.e., perfect output coupling—but we include an imperfect detector efficiency of $\eta = 0.9$ for optical detectors. In practice, η should be regarded as including all types of detection losses, including optical coupling losses.

Results for square pulses are presented here, although a variety of pulse shapes ranging from square waves to Gaussians gave strong entanglement and steering. Two different heat bath temperatures were chosen for comparison purposes: either with a cold reservoir at $T_{bath} = 200$ mK, or a “warm” reservoir of $T_{bath} = 4$ K. In both cases, the initial mechanical occupation number was chosen as $\bar{n}_{m,0} = 0.7$, corresponding to an initial precooled oscillator temperature of 200 mK. In the case of these optical simulations, we note that $dW_{ext}^{in} = dW_o^{in}$, since we assumed there were no internal loss mechanisms, and the optical thermal occupation is assumed to be negligible.

2. Entanglement results

The resulting predictions for entanglement in the case of the optomechanical parameters are plotted in Fig. 5, where the solid lines indicate results for idealized measurements on the mechanical oscillator, and dotted lines the expected operational measurements using a readout pulse.

Using these entanglement signatures, we have simulated the robust asymmetric EPR entanglement recently predicted in Ref. [38], but without approximations. A graph of the predicted quantum entanglement at low and high temperature

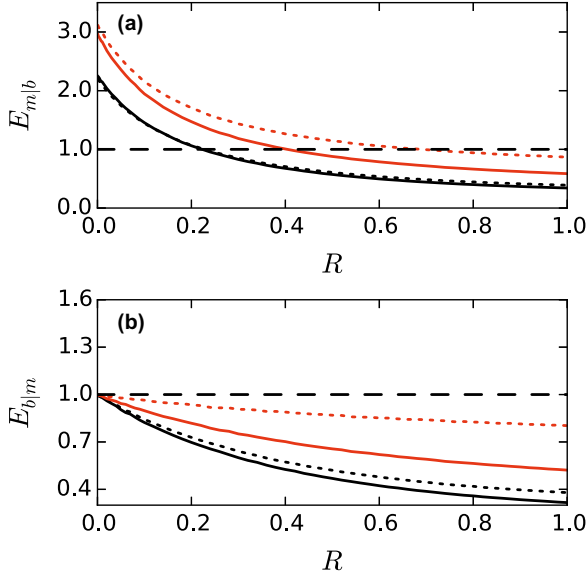


FIG. 6. (Color online) EPR steering vs entanglement gain parameter R , for the optomechanical conditions used in Fig. 5. Dashed lines indicate the result of using optical readouts, solid lines assume direct oscillator measurements. The lower black curves are for $T_{\text{bath}} = 200$ mK ($\bar{n}_{m,\text{th}} = 0.7$); the upper red (gray) curves are for $T_{\text{bath}} = 4$ K ($\bar{n}_{m,\text{th}} = 22.1$). (a) EPR steering of the mechanical system m is possible if $E_{m|b} < 1$. (b) EPR steering of the optical system is possible if $E_{b|m} < 1$. For both bath temperatures, two-way steering becomes possible once a threshold $R > R_0$ is reached.

is shown in Fig. 5 for two experimental scenarios. These calculations simulate the parameter regime of experiments on Si optomechanical crystal structures [2].

Further, we are able to establish the validity of the linearization assumptions, and agreement between the exact positive- P representation and the approximate Wigner method, for both optical and microwave experimental parameter values. Our investigation tells us that nonlinear quantum noise and deviation between exact positive P and approximate methods come into play only for stronger couplings, with $\chi_0 \sim \gamma_o$.

The physical interpretation of the results of Fig. 5 is that for any given initial mechanical oscillator occupation number $\bar{n}_{m,0}$, we can always obtain entanglement for $R = \int_0^t G(t') dt' > 0$, provided one uses the asymmetric criteria (4.3) and selects an optimal choice of both phase θ and gain factor g (4.4). This means we can in principle detect entanglement in the presence of thermal mechanical decoherence, without the need to use laser cooling to reduce the value of $\bar{n}_{m,0}$. Figure 5 indicates entanglement at a temperature $T_{\text{bath}} = 4$ K ($\bar{n}_{m,\text{th}} = 22.1$), provided the oscillator is precooled to $T_0 = 200$ mK ($\bar{n}_{m,0} \sim 0.7$). This is sensitive to the occupation number $\bar{n}_{m,\text{th}}$ of the mechanical heat bath but is more robust to thermal effects than using the symmetric criterion in Ref. [12].

3. EPR-steering results

Predictions for optomechanical EPR-steering experiments are presented in Fig. 6. The efficiency assumed here is $\eta = 0.9$. Generally, these simulations have more favorable

conditions for EPR steering, due to the relatively lower thermal occupations for optical inputs as compared to microwave inputs, even assuming the same temperatures. A thermal barrier can still exist for this paradox however.

The results show that the mechanical oscillator is steerable by the optical pulse system when $R > R_0$, where a minimum strength R_0 of the gain parameter required for a given $\bar{n}_{m,0}$. A thermal barrier means that a threshold level of pulse-oscillator interaction is required for a given initial thermal occupation $\bar{n}_{m,0}$ of the mechanical oscillator.

An EPR paradox can also be shown the other way, in which we steer the photons, not the massive oscillator, by the criterion

$$E_{b|m} = 4\Delta(\hat{X}_b - g\hat{X}_m^\phi)\Delta(\hat{P}_b + g\hat{P}_m^\phi) < 1. \quad (5.5)$$

Figure 4 shows that this is possible for any value of initial oscillator noise $\bar{n}_{m,0}$, and for any gain. There is no equivalent thermal barrier for the optical pulse “steered” by measurements made on the mechanical system, if the entangling pulse is not thermally excited. We also find that $E_{b|m}$ is less sensitive to mechanical decoherence. This is because we can select optimal gain values g to reduce the effect of the initial thermal noises $\bar{n}_{m,0}$ and the mechanical heat bath $\bar{n}_{m,\text{th}}$. The graphed results also calculate the externally measured criteria, $E_{b|r}$ and $E_{r|b}$, using pulse-probe methods, with reduced correlations.

C. Numerical methods

A semi-implicit interaction picture stochastic integration method was used [46], with 8×10^5 trajectories for positive- P simulations, up to 2×10^5 for the truncated Wigner simulations, and 10^4 total time steps. The two different phase-space methods gave identical results for these parameter values, apart from typical sampling errors with relative errors in the mean of up to ± 0.01 , and hence only one line is plotted for both methods. Truncation errors due to the finite time step were verified to be less than the sampling errors. To minimize software or hardware errors, independent computer codes were written and tested in different languages (C++ and SCILAB) and with different computer hardware, both using double precision floating point. These gave identical results in all cases tested.

VI. SUMMARY

Optomechanics presents a challenge for exact quantum simulations. It combines a range of occupation numbers and time scales with nonequilibrium and nonlinear open system quantum dynamics. These results demonstrate that the positive- P representation approach can give a useful first principles simulation of the standard model in the quantum regime [30]. For the parameters simulated here, the truncated Wigner approach is also reliable and simple to implement. This method needs to be verified by the more precise positive- P simulations for strong couplings. To the extent we can make comparisons, our results also verify previous analyses using adiabatic techniques.

These simulation techniques can be readily scaled up to study multipartite systems with many oscillator modes [37], strong interactions, and nonadiabatic behavior. Our main result in this work illustrates a fundamental physical principle: *inferred changes to a massive system as a result of*

measurement at a distant site will be inhibited by thermal noise. We note that the reverse type of inference is not inhibited, which is typical of the directional property of EPR-steering inference. It suggests that the mechanism for the apparent directional property of quantum measurement could be fundamentally related to noise sources. Direct observation of two-way EPR inference for a massive system is therefore an important next goal in nanomechanics.

ACKNOWLEDGMENTS

We acknowledge support from the Australian Research Council via Discovery and DECRA grants. This work was also supported in part by the National Science Foundation under Grant No. PHYS-1066293 and the hospitality of the Aspen Center for Physics. We thank Palomaki *et al.* for details of their experiment.

APPENDIX: EFFECT OF LOSSES AND INEFFICIENCIES

In the detection of either optical or microwave fields, we assume that external detection is carried out with finite efficiency η . Unless stated otherwise, optical detection efficiencies are assumed to be at $\eta = 0.9$, while microwave photons are assumed detected with $\eta = 0.2$, as reported experimentally.

In order to take this into account, we use a simple model, in which detector inefficiency is modeled as a beam splitter that allows only some of the incident photons to reach the detector. For consistency, one must include a vacuum input so that commutation relations are still valid. This gives

$$\hat{a}_k^d = \sqrt{\eta}\hat{a}_k + \sqrt{1-\eta}\hat{a}_k^v,$$

where \hat{a}^d means the detected amplitude, \hat{a}^v means the vacuum amplitude that is input to the beam splitter, and $k = [b, r]$ as previously. As the inefficiency terms are often combined with gain terms, because these effects compensate each other, we define $\Gamma \equiv (1 - \eta)(1 + g^2)$.

This model yields for the detected quadratures

$$\begin{aligned}\hat{X}_k^d &= \sqrt{\eta}\hat{X}_k + \sqrt{1-\eta}\hat{X}_k^v, \\ \hat{P}_k^d &= \sqrt{\eta}\hat{P}_k + \sqrt{1-\eta}\hat{P}_k^v.\end{aligned}$$

The variance terms corresponding to differences of quadratures in two beams now become

$$\begin{aligned}\sigma^2 &= \langle (\hat{X}_r^d - g\hat{X}_b^d)^2 \rangle \\ &= \frac{\Gamma}{4} + \eta \langle (\hat{X}_r - g\hat{X}_b)^2 \rangle.\end{aligned}$$

1. Entanglement criteria

For the additive entanglement criterion at unit gain, the inclusion of detector inefficiency in the calculation gives entanglement if $\Delta_{\text{ent}}^a < 1$, where

$$\Delta_{\text{ent}}^a = (1 - \eta) + \eta \{ \Delta^2(\hat{X}_r + \hat{X}_b) + \Delta^2(\hat{P}_r - \hat{P}_b) \}.$$

Including gain, the product criterion indicates entanglement, if $\Delta_{\text{ent}}^p < 1$, where

$$\begin{aligned}\Delta_{\text{ent}}^p &= (1 - \eta) \left[1 + 16\eta^2 \frac{\Delta^2(\hat{X}_r + g\hat{X}_b)\Delta^2(\hat{P}_r - g\hat{P}_b)}{\Gamma^2} \right. \\ &\quad \left. + 4\eta \frac{[\Delta(\hat{X}_r + g\hat{X}_b)]^2 + [\Delta(\hat{P}_r - g\hat{P}_b)]^2}{\Gamma} \right]^{\frac{1}{2}}.\end{aligned}$$

2. EPR-steering criteria

Similarly, the *measured* EPR-steering criteria including detection inefficiency become $E_{r|b}^2 < 1$ where

$$\begin{aligned}E_{r|b}^2 &= \Gamma^2 + 16\eta^2 \Delta^2(\hat{X}_r + g\hat{X}_b)\Delta^2(\hat{P}_r - g\hat{P}_b) \\ &\quad + 4\eta\Gamma[\Delta^2(\hat{X}_r + g\hat{X}_b) + \Delta^2(\hat{P}_r - g\hat{P}_b)]\end{aligned}$$

and $r \leftrightarrow b$ for the other steering direction. We note that this is much harder to satisfy when $\eta < 1$ than in the perfect efficiency case. The physical reason is simply that the injection of uncorrelated vacuum noise through the inefficient detection process tends to reduce the strong correlation required to observe an EPR paradox in these experiments.

-
- [1] A. D. O'Connell *et al.*, *Nature (London)* **464**, 697 (2010).
[2] J. Chan *et al.*, *Nature (London)* **478**, 89 (2011).
[3] S. Groblacher *et al.*, *Nat. Phys.* **5**, 485 (2009).
[4] J. D. Teufel *et al.*, *Nature (London)* **475**, 359 (2011); **471**, 204 (2011).
[5] A. H. Safavi-Naeini, J. Chan, J. T. Hill, T. P. M. Alegre, A. Krause, and O. Painter, *Phys. Rev. Lett.* **108**, 033602 (2012).
[6] N. Brahms, T. Botter, S. Schreppler, D. W. C. Brooks, and D. M. Stamper-Kurn, *Phys. Rev. Lett.* **108**, 133601 (2012).
[7] T. J. Kippenberg and K. J. Vahala, *Science* **321**, 1172 (2008).
[8] M. Aspelmeyer *et al.*, *J. Opt. Soc. Am. B* **27**, A189 (2010).
[9] T. A. Palomaki *et al.*, *Science* **342**, 710 (2013).
[10] V. Giovannetti, S. Mancini, and P. Tombesi, *Europhys. Lett.* **54**, 559 (2001); S. Mancini, V. Giovannetti, D. Vitali, and P. Tombesi, *Phys. Rev. Lett.* **88**, 120401 (2002).
[11] C. Genes, A. Mari, P. Tombesi, and D. Vitali, *Phys. Rev. A* **78**, 032316 (2008).
[12] S. G. Hofer, W. Wieczorek, M. Aspelmeyer, and K. Hammerer, *Phys. Rev. A* **84**, 052327 (2011).
[13] M. R. Vanner *et al.*, *Proc. Natl. Acad. Sci. USA* **108**, 16182 (2011); I. Pikovski *et al.*, *Nat. Phys.* **8**, 393 (2012).
[14] A. Einstein, B. Podolsky, and N. Rosen, *Phys. Rev.* **47**, 777 (1935).
[15] M. D. Reid, *Phys. Rev. A* **40**, 913 (1989).
[16] M. D. Reid *et al.*, *Rev. Mod. Phys.* **81**, 1727 (2009).
[17] E. Schrödinger, *Naturwissenschaften* **23**, 844 (1935).
[18] W. Marshall, C. Simon, R. Penrose, and D. Bouwmeester, *Phys. Rev. Lett.* **91**, 130401 (2003).
[19] M. Born, *Born-Einstein Letters, 1916–1955: Friendship, Politics and Physics in Uncertain Times* (Palgrave MacMillan, Basingstoke, 2005).

- [20] E. Schrödinger, *Proc. Cambridge Philos. Soc.* **31**, 555 (1935); **32**, 446 (1936).
- [21] H. M. Wiseman, S. J. Jones, and A. C. Doherty, *Phys. Rev. Lett.* **98**, 140402 (2007); S. J. Jones, H. M. Wiseman, and A. C. Doherty, *Phys. Rev. A* **76**, 052116 (2007).
- [22] E. G. Cavalcanti, S. J. Jones, H. M. Wiseman, and M. D. Reid, *Phys. Rev. A* **80**, 032112 (2009).
- [23] P. D. Drummond and C. W. Gardiner, *J. Phys. A: Math. Gen.* **13**, 2353 (1980).
- [24] M. K. Olsen, A. B. Melo, K. Dechoum, and A. Z. Khoury, *Phys. Rev. A* **70**, 043815 (2004).
- [25] L. M. Duan, G. Giedke, J. I. Cirac, and P. Zoller, *Phys. Rev. Lett.* **84**, 2722 (2000).
- [26] E. P. Wigner, *Phys. Rev.* **40**, 749 (1932); J. E. Moyal, *Proc. Cambridge Philos. Soc.* **45**, 99 (1949); R. Graham, in *Springer Tracts in Modern Physics: Quantum Statistics in Optics and Solid-State Physics*, edited by G. Hohler (Springer, New York, 1973); P. Kinsler and P. D. Drummond, *Phys. Rev. A* **43**, 6194 (1991).
- [27] P. D. Drummond and A. D. Hardman, *Europhys. Lett.* **21**, 279 (1993).
- [28] M. D. Reid and P. D. Drummond, *Phys. Rev. A* **40**, 4493 (1989); P. D. Drummond and M. D. Reid, *ibid.* **41**, 3930 (1990).
- [29] S. Chaturvedi, K. Dechoum, and P. D. Drummond, *Phys. Rev. A* **65**, 033805 (2002); K. Dechoum, P. D. Drummond, S. Chaturvedi, and M. D. Reid, *ibid.* **70**, 053807 (2004).
- [30] A. F. Pace, M. J. Collett, and D. F. Walls, *Phys. Rev. A* **47**, 3173 (1993).
- [31] M. Ludwig, B. Kubala, and F. Marquardt, *New J. Phys.* **10**, 095013 (2008); M. Ludwig, A. H. Safavi-Naeini, O. Painter, and F. Marquardt, *Phys. Rev. Lett.* **109**, 063601 (2012).
- [32] A. Kronwald, M. Ludwig, and F. Marquardt, *Phys. Rev. A* **87**, 013847 (2013).
- [33] P. Deuar and P. D. Drummond, *Phys. Rev. Lett.* **98**, 120402 (2007).
- [34] B. Opanchuk *et al.*, *Phys. Lett. A* **378**, 946 (2014).
- [35] L. Qiu, L. Gan, W. Ding, and Z.-Y. Li, *J. Opt. Soc. Am. B* **30**, 1683 (2013).
- [36] S. Lloyd, *Science* **273**, 1073 (1996).
- [37] J. Chan *et al.*, *Appl. Phys. Lett.* **101**, 081115 (2012).
- [38] Q. Y. He and M. D. Reid, *Phys. Rev. A* **88**, 052121 (2013).
- [39] V. Händchen *et al.*, *Nat. Photon.* **6**, 596 (2012); S. L. W. Midgley, A. J. Ferris, and M. K. Olsen, *Phys. Rev. A* **81**, 022101 (2010); J. Bowles, T. Vértesi, M. T. Quintino, and N. Brunner, *Phys. Rev. Lett.* **112**, 200402 (2014).
- [40] V. B. Braginsky and A. B. Manukin, *Sov. Phys. JETP* **25**, 653 (1967); A. Dorsel, J. D. McCullen, P. Meystre, E. Vignes, and H. Walther, *Phys. Rev. Lett.* **51**, 1550 (1983).
- [41] H. J. Carmichael, *Statistical Methods in Quantum Optics I: Master Equations and Fokker-Planck Equations* (Springer, Berlin, 2002).
- [42] B. Yurke, *Phys. Rev. A* **32**, 300 (1985); C. W. Gardiner and M. J. Collett, *ibid.* **31**, 3761 (1985).
- [43] A. Gilchrist, C. W. Gardiner, and P. D. Drummond, *Phys. Rev. A* **55**, 3014 (1997).
- [44] P. D. Drummond and M. Hillery, *The Quantum Theory of Nonlinear Optics* (Cambridge University Press, Cambridge, 2014).
- [45] S. Chaturvedi and P. D. Drummond, *Eur. Phys. J. B* **8**, 251 (1999).
- [46] P. D. Drummond and I. K. Mortimer, *J. Comp. Phys.* **93**, 144 (1991).
- [47] S. M. Tan, *Phys. Rev. A* **60**, 2752 (1999).
- [48] V. Giovannetti, S. Mancini, D. Vitali, and P. Tombesi, *Phys. Rev. A* **67**, 022320 (2003).
- [49] M. D. Reid, *Phys. Rev. A* **88**, 062108 (2013); W. Bowen *et al.*, *Phys. Rev. Lett.* **90**, 043601 (2003).